 ICCES, vol.13, no.2, pp.35-41

Nonlinear third-order shear deformation FE simulation of the sensor output voltage of piezolaminated plates

Thang Duy Vu, Ruediger Schmidt[1]

Summary

Two geometrically nonlinear finite plate elements incorporating piezoelectric layers are presented, based either on first- or third-order shear deformation theory. Numerical tests are performed for the sensor output voltage of a piezolaminated plate.

keywords: Nonlinear FE analysis, piezolaminated plate, third-order shear deformation

Introduction

For the numerical simulation of piezointegrated thin structures many suggestions ranging from geometrically linear [Crawley, E.F. & de Luis, J. (1987); Lammering, R. (1991)] to geometrically nonlinear [Chróścielewski, J., Klosowski, P. & Schmidt, R (1998); Mukherjee, A. & Chaudhuri, A.S. (2002); Lentzen, S. & Schmidt, R. (2004)] beam and shell elements have been made. In the latter paper we have shown the importance of geometrically nonlinear analysis, especially when the sensing capabilities of the piezoelectric layers are investigated. In this paper linear and nonlinear dynamic analysis is performed based on first- and third-order shear deformation plate theory.

Strain-displacement relations

First-order shear deformation theory

The results presented in this work, which refer to the first-order shear deformation theory (FOSD) or Reissner-Mindlin hypothesis, are based on the von Kármán-type nonlinearity. The FOSD hypothesis for the through-thickness variation of the tangential and normal displacement components reads

$$v_\alpha = \overset{0}{v}_\alpha + \Theta^3 \overset{1}{v}_\alpha, \quad v_3 = \overset{0}{v}_3 \tag{1}$$

where the mid-surface displacements are denoted by 0 and the rotations by 1.

The Green-Lagrange strain components for the nonlinear von Kármán-type FOSD plate element can be expressed as:

$${}_0\varepsilon_{\alpha\beta} = \overset{0}{\varepsilon}_{\alpha\beta} + \Theta^3 \overset{1}{\varepsilon}_{\alpha\beta}, \quad {}_0\varepsilon_{\alpha 3} = \overset{0}{\varepsilon}_{\alpha 3}, \quad {}_0\varepsilon_{33} = 0 \tag{2}$$

The constant terms, denoted by 0 and the linear terms, denoted by 1 are determined as

$$\overset{0}{\varepsilon}_{\alpha\beta} = \frac{1}{2}\left(\overset{0}{v}_{\alpha|\beta} + \overset{0}{v}_{\beta|\alpha} + \underline{\overset{0}{v}_{3,\alpha}\overset{0}{v}_{3,\beta}}\right), \quad \overset{1}{\varepsilon}_{\alpha\beta} = \frac{1}{2}\left(\overset{1}{v}_{\alpha|\beta} + \overset{1}{v}_{\beta|\alpha}\right), \tag{3}$$

[1]Iam, Rwth Aachen, Germany.

$$\overset{0}{\varepsilon}_{\alpha 3} = \frac{1}{2}\left(\overset{0}{v}_{3,\alpha} + \overset{1}{v}_{\alpha}\right)$$

where the nonlinear term is underlined.

First-order shear deformation theory

The results referring to the third-order shear deformation theory (TOSD) are obtained with a finite plate element developed by [Nguyen, Q.D., Lentzen, S. & Schmidt, R (2004)]. The finite element is based on the von Kármán-type nonlinearity, too. The TOSD hypothesis for the through-thickness variation of the tangential and normal displacement components reads

$$v_{\alpha} = \overset{0}{v}_{\alpha} + \Theta^3 \overset{1}{v}_{\alpha} + \left(\Theta^3\right)^2 \overset{2}{v}_{\alpha} + \left(\Theta^3\right)^3 \overset{3}{v}_{\alpha}, \quad v_3 = \overset{0}{v}_3 \tag{4}$$

where the constant, linear, quadratic and cubic terms are denoted by 0, 1, 2 and 3, respectively. The Green-Lagrange strain components for the von Kármán-type nonlinearity TOSD plate element can be expressed as:

$${}_0\varepsilon_{\alpha\beta} = \overset{0}{\varepsilon}_{\alpha\beta} + \Theta^3 \overset{1}{\varepsilon}_{\alpha\beta} + \left(\Theta^3\right)^3 \overset{3}{\varepsilon}_{\alpha\beta}, \quad {}_0\varepsilon_{\alpha 3} = \overset{0}{\varepsilon}_{\alpha 3} + \left(\Theta^3\right)^2 \overset{2}{\varepsilon}_{\alpha 3}, \quad {}_0\varepsilon_{33} = 0 \tag{5}$$

where

$$\begin{aligned} &\overset{0}{\varepsilon}_{\alpha\beta} = \frac{1}{2}\left(\overset{0}{v}_{\alpha|\beta} + \overset{0}{v}_{\beta|\alpha} + \underline{\overset{0}{v}_{3,\alpha}\overset{0}{v}_{3,\beta}}\right), \quad \overset{1}{\varepsilon}_{\alpha\beta} = \frac{1}{2}\left(\overset{1}{v}_{\alpha|\beta} + \overset{1}{v}_{\beta|\alpha}\right), \\ &\overset{3}{\varepsilon}_{\alpha\beta} = -\frac{2}{3h^2}\left(\overset{1}{v}_{\alpha|\beta} + \overset{1}{v}_{\beta|\alpha} + 2\overset{0}{v}_{3|\alpha\beta}\right) \end{aligned} \tag{6}$$

and

$$\overset{0}{\varepsilon}_{\alpha 3} = \frac{1}{2}\left(\overset{1}{v}_{\alpha} + \overset{0}{v}_{3,\alpha}\right), \quad \overset{2}{\varepsilon}_{\alpha 3} = -\frac{2}{h^2}\left(\overset{1}{v}_{\alpha} + \overset{0}{v}_{3,\alpha}\right) \tag{7}$$

The cubic term of the tangential strains (denoted by 3) is neglected in the numerical applications.

Numerical Method

According to the virtual work principle, for a state of equilibrium the internal virtual work δWi is equal to the external virtual work δWe. As a continuation of earlier work done by Palmerio et al. (1990) and Kreja et al. (1995) in the present work a total Lagrangian approach is chosen. Consequently, the second Piola-Kirchhoff stress and Green-Lagrange strains are chosen as the mechanical quantities. The electric field vector referring to the undeformed configuration is calculated as the negative gradient of the electric potential ϕ along the undeformed surface parameters Θ^i

$${}_0E_i = -\frac{\partial \phi}{\partial \Theta^i} \tag{8}$$

The mechanical and electrical quantities are coupled to each other by two constitutive equations, namely the direct and the converse piezoelectric effect

$$\{{}_0D\} = [e]\{{}_0\varepsilon\} + [\delta]\{{}_0E\}, \quad \{{}_0S\} = [c]\{{}_0\varepsilon\} - [e]^T\{{}_0E\} \tag{9}$$

where $\{{}_0S\}$ denotes the stress vector, $\{{}_0\varepsilon\}$ the strain vector, $\{{}_0D\}$ the electric displacement vector and $\{{}_0E\}$ the electric field vector

$$\{{}_0S\} = \begin{Bmatrix} \sigma^{11} \\ \sigma^{22} \\ \tau^{12} \\ \tau^{23} \\ \tau^{13} \end{Bmatrix}, \quad \{{}_0\varepsilon\} = \begin{Bmatrix} \varepsilon_{11} \\ \varepsilon_{22} \\ 2\varepsilon_{12} \\ 2\varepsilon_{23} \\ 2\varepsilon_{13} \end{Bmatrix}, \quad \{{}_0D\} = \begin{Bmatrix} D^1 \\ D^2 \\ D^3 \end{Bmatrix}, \quad \{{}_0E\} = \begin{Bmatrix} E_1 \\ E_2 \\ E_3 \end{Bmatrix}. \tag{10}$$

Further $[e] = [d][c]$ and $[e]^T = [c][d]^T$, where [c] denotes the elasticity matrix for anisotropic materials, $[d]$ the piezoelectric constant matrix and $[\delta]$ the dielectric constant matrix

$$[c] = \begin{bmatrix} c_{11} & c_{12} & c_{13} & 0 & 0 \\ c_{12} & c_{22} & c_{23} & 0 & 0 \\ c_{13} & c_{23} & c_{33} & 0 & 0 \\ 0 & 0 & 0 & c_{44} & c_{45} \\ 0 & 0 & 0 & c_{45} & c_{55} \end{bmatrix}, \quad [d]^T = \begin{bmatrix} 0 & 0 & d_{31} \\ 0 & 0 & d_{31} \\ 0 & 0 & 0 \\ 0 & d_{15} & 0 \\ d_{15} & 0 & 0 \end{bmatrix}, \tag{11}$$

$$[\delta] = \begin{bmatrix} \delta_{11} & 0 & 0 \\ 0 & \delta_{22} & 0 \\ 0 & 0 & \delta_{33} \end{bmatrix}$$

If it is further assumed that the electric field is homogeneously distributed over the electrode pair, only one additional degree of freedom has to be introduced per electrode pair, namely the electric potential. After introducing the principle of virtual work, the differential equations of motion to be solved are

$$[M]\{\ddot{q}\} + \{F_i\} = \{F_e\} \quad , \quad \{Q_i\} = \{Q_e\} \tag{12}$$

where $[M]$ denotes the mass matrix and $\{q\}$ are the generalized nodal displacements. The in-balance nodal force and electrode charge vectors are denoted by $\{F_i\}$ and $\{Q_i\}$, respectively. The externally applied force and charge vectors are denoted by the right subscript e. The electric potentials are calculated from the equilibrium between the mechanically and the electrically induced in-balance charges.

Numerical Examples

The numerical example deals with a fully clamped plate with a PZT sensor as depicted in figure 1, see [Yi, S., Ling, S. F. and Ying, M. (2000)]. The material parameters are E=197GPa, ν = 0.33 and ρ = 7900 kg/m^3. The load consists of a uniform step pressure of $2{\cdot}10^4$ Pa. The transient analysis is performed with a quarter of the plate with a mesh of [5x5] and a time step of $\Delta t = 2{\cdot}10^{-7}$ s to satisfy space and time resolution requirements.

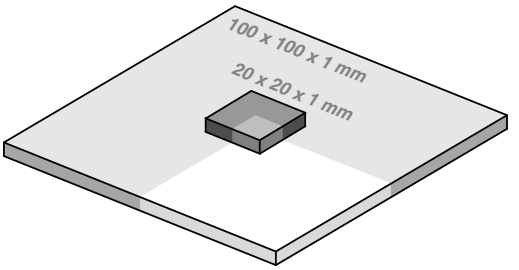

Figure 1: Clamped piezolaminated plate

Figs. 2 and 3 display the results for the mid-point displacement and the sensor output voltage. It can be seen that the TOSD results agree very well with the FOSD theory.

It can be expected that for thicker structures the deflection of TOSD plates differs more from FOSD plates, than for thinner structures. Therefore, the above example has been altered using the same structure but now with a thickness of 5 mm. Due to the higher thickness of the plate, a higher pressure has to be applied to obtain transverse deflections in the same order of magnitude of those obtained for the thinner plate. In this case, a pressure of $2{\cdot}10^5$ Pa was applied. The results are displayed in Figure 4 and 5.

Conclusions

In this work two geometrically nonlinear, von Kármán type plate elements are discussed, based on the first- and third-order transverse shear deformation theory, respectively. By means of several numerical examples it has been shown that in geometrically linear as well as geometrically nonlinear deformations the results obtained by both finite elements start diverging when the structure becomes thicker. The importance of geometrically nonlinear effects, especially for sensor applications, has been demonstrated.

References

1. **Chróścielewski, J., Klosowski, P. & Schmidt, R.** (1998): Theory and numerical simulation of nonlinear vibration control of arches with piezoelectric distributed actuators. *Machine Dynamics Problems* , 20, 73-90.

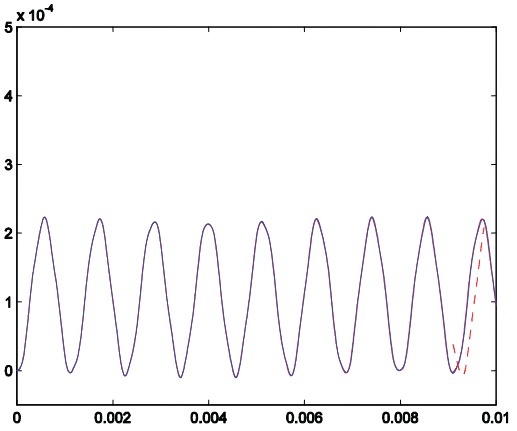

Figure 2: Mid-point displacement of the clamped plate

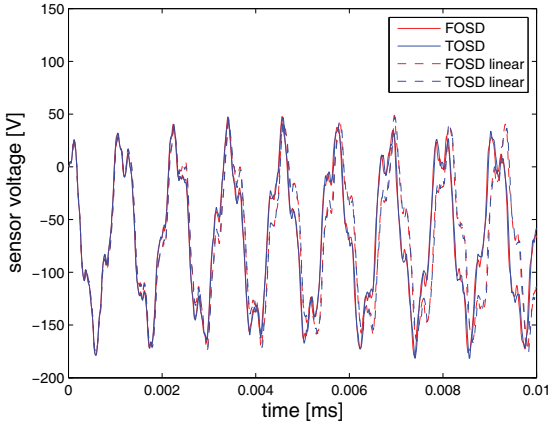

Figure 3: Sensor voltage of the clamped plate

2. **Crawley, E.F. & de Luis, J.** (1987): Use of piezoelectric actuators as elements of intelligent structures, *AIAA Journal*, 25(10), 1373-1385.

3. **Kioua, H. & Mirza, S.** (2000): Piezoelectric induced bending and twisting of laminated composite shallow shells. *Smart Mater. Struct*., 6, 476-484.

4. **Kreja, I. & Schmidt, R**. (1995): Moderate rotation shell theory in FEM application. *Zeszyty Naukowe Politechniki Gdańskiej* (Research Transactions of Gdansk University of Technology), 522, 229-249.

5. **Lammering, R.** (1991): The application of finite shell elements for composites containing piezoelectric polymers in vibration control. *Computers & Structures*, 41, 1101-1109.

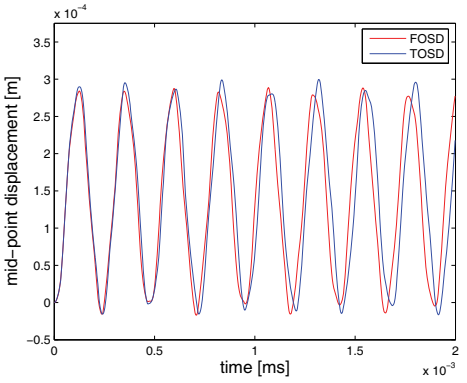

Figure 4: Mid-point displacement of the clamped thick plate

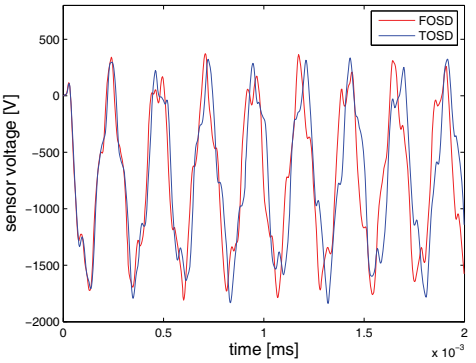

Figure 5: Sensor voltage of the clamped thick plate

6. **Lee, S., Goo, N.S., Park, H.C., Yoon, K.J. & Cho, C.** (2003): A nine-node assumed strain shell element for analysis of a coupled electromechanical system. *Smart Mater. Struct.*, 12, 355-362.

7. **Lentzen, S. & Schmidt, R.** (2004): Simulation of sensor application and shape control of piezoelectric structures at large deflections, in: *Advances in Computational & Experimental Engineering & Science,* eds. Atluri, S.N. & Tadeu, A.J.B., Tech Science Press, 439-444.

8. **Mukherjee, A. & Chaudhuri, A.S.** (2002): Piezolaminated beams with large deformations. *Int. J. of Solids and Structures*, 14, 1567-1582.

9. **Nguyen, Q.D., Lentzen, S. & Schmidt, R** (2004): A geometrically nonlinear third-order shear deformation finite plate element incorporating piezoelectric layers, *Proc. ICMT2004*

10. **Palmerio, A.F., Reddy, J.N. & Schmidt, R**. (1990): On a moderate rotation

theory of laminated anisotropic shells – part 2. finite-element analysis, *Int. J. Non-Linear Mechanics*, 25(6), 701-714.

11. **Piefort, V**. (2001): *Finite element modeling of piezoelectric active structures*, PhD Thesis, 2001, Université Libre de Bruxelles.
12. **Yi, S., Ling, S. F. and Ying, M.** (2000): Large deformation finite element analyses of composite structures integrated with piezoelectric sensors and actuators. *Finite Elements in Analysis and Design*, 35, pp. 1–15.